

Pyrrrolizine fused ambipolar PAHs as a new strategy towards the efficient red and NIR emissive dyes.

Krzysztof Bartkowski,^{‡,[a]} Abhishek Kumar Gupta,^{‡,[b]} Tomas Matulaitis^[b], Maja Morawiak^[a], Eli Zysman-Colman,^{*[b]} and Marcin Lindner^{*[a]}

General information

All reagents and solvents were purchased from commercial sources and were used as received unless otherwise noted. Reagent grade solvents (CH₂Cl₂, hexane) were distilled prior to use. For water-sensitive reactions solvents were dried using Solvent Purification System from MBraun. Transformations with moisture and oxygen sensitive compounds were performed under a stream of argon. The reaction progress was monitored by means of thin layer chromatography (TLC), which was performed on aluminum foil plates, covered with Silica gel 60 F254 (Merck). Products purification was done by means of column chromatography with Kieselgel 60 (Merck). The identity and purity of prepared compounds were proved by ¹H NMR and ¹³C NMR spectrometry as well as by MS spectrometry (via EI-MS) and IR spectroscopy. NMR spectra were measured on Bruker AM 500 MHz, Bruker AM 600 MHz or Varian 600 MHz instruments with TMS as internal standard. Chemical shifts for ¹H NMR are expressed in parts per million (ppm) relative to tetramethylsilane (δ 0.00 ppm), CDCl₃ (δ 7.26 ppm) or CD₂Cl₂ (δ 5.32 ppm). Chemical shifts for ¹³C NMR are expressed in ppm relative to CDCl₃ (δ 77.16 ppm) or CD₂Cl₂ (δ 54.00 ppm). Data are reported as follows: chemical shift, multiplicity (s = singlet, d = doublet, dd = doublet of doublets, t = triplet, m = multiplet), coupling constant (Hz), and integration. EI/ESI/APCI mass spectra were obtained on AutoSpec Premier spectrometer. IR spectra were recorded on JASCO FT/IR-6200 spectrometer.

DFT Calculations

The Density functional theory (DFT) calculations, including geometry optimization with a subsequent frequency calculation of the emitters, were implemented using by the Silico software 3.1.0 package manages calculations submitted to Gaussian (2016 + C.01),¹⁻⁷ in the gas phase using Density Functional Theory (DFT) with the PBE0 functional⁸ and the 6-31G(d,p) basis set, starting with the molecular geometry⁹ obtained from single crystal X-ray diffraction analysis. Excited singlet and triplet states were calculated by performing time-dependent DFT (TD-DFT) calculations within the Tamm-Dancoff approximation using the same functional and basis set.^{10,11}

The MICD calculations were performed by using the AIMAll¹² software based on GIAO analysis of the optimized geometry of compounds **3a** and **3b** (B3LYP,¹³ 6-311G++(d,p)) or non-modified crystal geometry for **1** and **3c**. The GIAO analysis was performed with Gaussian (2016.A.01).

Electrochemistry

Cyclic Voltammetry (CV) and Differential pulse voltammetry (DPV) analysis were performed on an Electrochemical Analyzer potentiostat model 620E from CH Instruments. Samples were prepared in dichloromethane (DCM) solutions, which were degassed by sparging with DCM-saturated nitrogen gas for 5 minutes prior to measurements. All measurements were performed using 0.1M tetra-*n*-butylammonium hexafluorophosphate, [^{*n*}Bu₄N]PF₆, as an electrolyte, in DCM at scan rate of 100 mV s⁻¹. An Ag/Ag⁺ electrode was used as the reference electrode, a glassy carbon electrode was used as the working electrode and a platinum wire was used as the counter electrode. The redox potentials are reported relative to a saturated calomel electrode (SCE) with a ferrocene/ferrocenium/ (F_c/F_c⁺) redox couple as the internal standard (0.46 V vs SCE).¹⁴ The HOMO and LUMO energies were determined using $E_{HOMO/LUMO} = -(E^{ox}/E^{red} + 4.8)eV$,¹⁵ where E^{ox} is anodic peak potential and E^{red} is cathodic peak potential determined from DPV relative to F_c/F_c⁺.

Photophysical measurements

Sample preparation

Two types of samples were used: dilute solutions and doped films (solid state). Solution samples were prepared using HPLC-grade solvents with varying concentrations on the order of 5×10^{-5} M for emission studies. Quartz cuvettes were used for all solution-state photophysics measurements. Aerated solutions were prepared by bubbling with compressed air for 5 minutes whereas degassed solutions were prepared via three freeze-pump-thaw cycles prior to emission and lifetime analysis using an in-house adapted fluorescence cuvette, itself purchased from Starna. Doped films were prepared by spin-coating 50 μ L of 20 mg mL⁻¹ solution in chloroform (5 wt.% of emitter in CBP) (chloroform obtained from Sigma Aldrich, HPLC grade) at 2000 RPM in ambient environment on quartz substrates and were annealed at 75 °C for 10 min.

UV/Vis Absorption

Absorption spectra were recorded at RT using a Shimadzu UV-2600 double beam spectrophotometer. Molar absorptivity determination was verified by linear least-squares fit of values obtained from at least four independent solutions at varying concentrations with absorbance ranging from 1.4×10^{-5} to 9.1×10^{-6} mol mL⁻¹ for **1**, 2.3×10^{-5} to 8.5×10^{-6} mol mL⁻¹ for **3a**, 1.5×10^{-5} to 9.4×10^{-6} mol mL⁻¹ for **3b**, and 1.1×10^{-5} to 7.0×10^{-6} mol mL⁻¹ for **3c**.

Steady-state emission and time-resolved PL decay

Steady-state and time-resolved emission spectra were recorded at 298 K using an Edinburgh Instruments FS5 fluorimeter in an oxygen-free atmosphere. Solution samples for the steady-state measurements were excited at 420-500 nm using a Xenon lamp and at 374 nm using a 5 mW EPL-375 diode laser (Edinburgh Instruments) for time-resolved measurements. Solid state samples for the steady-state were excited at 340 nm and at 374 nm for time-resolved measurements. Doped films were placed in a liquid nitrogen cryostat DN-V (Oxford Instruments) and were kept under vacuum of $<10^{-4}$ mbar. PL decays were measured using time-correlated single photon counting (TCSPC) mode and multi-channel scaling (MCS).

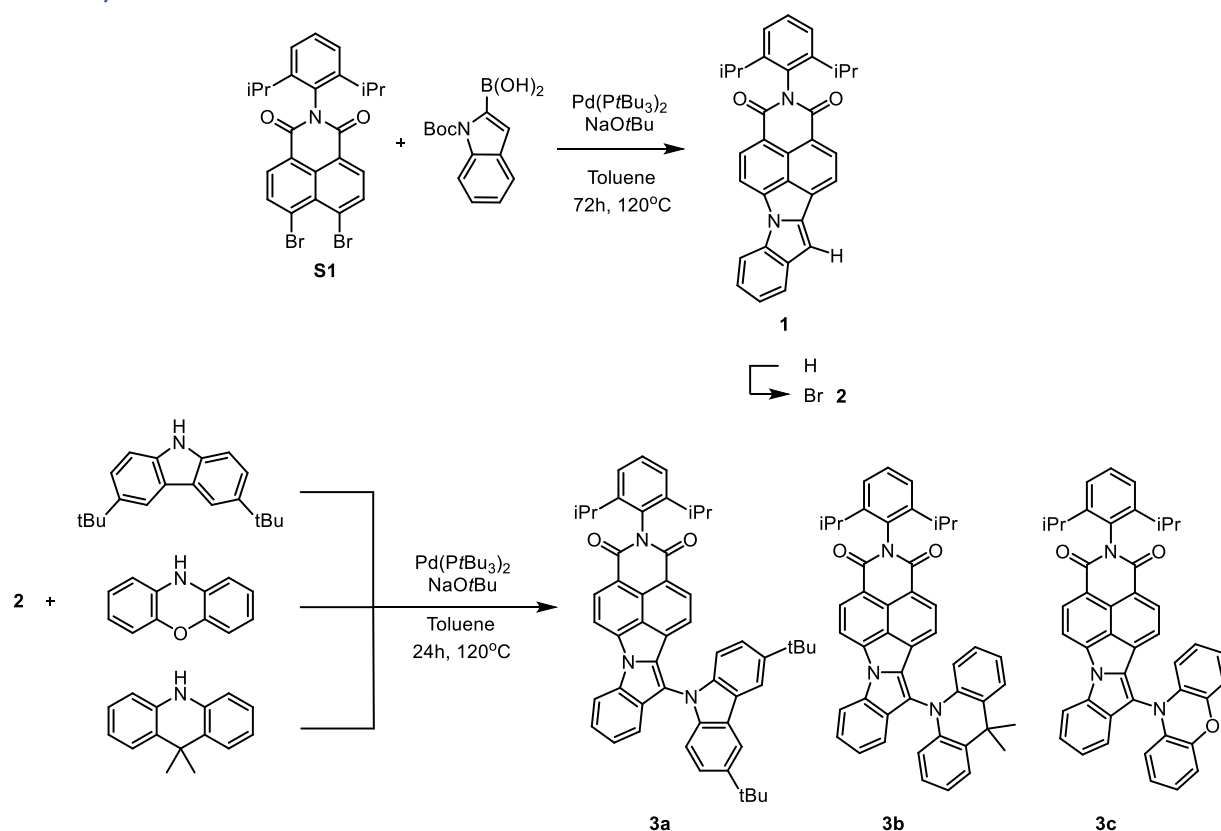
Photoluminescence quantum yields (PLQY)

Photoluminescence quantum yields for solutions were determined using the optically dilute method in which four sample solutions with absorbance of ca. 0.100, 0.075, 0.050 and 0.025 at 410 nm were used.^{16,17} Their emission intensities were compared with those of a reference, tris(2,2'-bipyridine)ruthenium(II) chloride, whose quantum yield (Φ_r) in H₂O was determined to be 2.8 % using absolute method.^{18,19} The quantum yield of the sample, Φ_{PL} , can be determined by the equation $\Phi_{PL} = \Phi_r(A_r/A_s)(I_s/I_r)(n_s/n_r)^2$, where A stands for the absorbance at the excitation wavelength ($\lambda_{exc} = 410$ nm), I is the integrated area under the corrected emission curve and n is the refractive index of the solvent with the subscripts "s" and "r" representing sample and reference respectively. The Beer-Lambert law was found to be linear at the concentrations of the solutions. For each sample, linearity between absorption and emission intensity was verified through linear regression analysis and additional measurements were acquired until the Pearson regression factor (R^2) for the linear fit of the data set surpassed 0.9. Individual relative quantum yield values were calculated for each solution and the values reported represent the gradient value.

A Hamamatsu C9920-02 integrating sphere was employed for PLQY measurements for thin film samples.²⁰ A xenon lamp coupled to a monochromator enabled selective excitation, chosen here to be 305 nm and 340 nm, for thin films. The output was then fed into the integrating sphere via a fibre,

exciting the sample. PL spectra were collected with a multimode fibre and detected with a back-thinned CCD under a nitrogen or oxygen atmosphere as required.

The synthesis



Synthesis of **S1** was done according to the reported protocol.²¹

(1) To a 25 mL Schlenk vessel **1** (100 mg, 0.194 mmol, 1 equiv.) and N-Boc-2-indoloboronic acid (66 mg, 0.252 mmol, 1.3 equiv.) were put with catalyst (Pd(PtBu₃)₂) (20 mg, 0.04 mmol, 0.2 equiv.) and NaOtBu (84 mg, 0.873 mmol, 4.5 equiv.) and dry on vacuum for 30 minutes. After this time toluene (6 mL) was added in argon atmosphere and the vessel was closed with a glass cap and put to the oil bath to stir in 120 °C. After 72 hours the solvent was evaporated, the residue was dissolved in DCM and washed with water (3x20 mL) and brine (20 mL). The organic phase was dried over Na₂SO₄. After removing the solvent mixture was subjected to a column chromatography (10% EtOAc/Hexane) to give product **2** (40%, 36 mg, pale yellow-orange solid). ¹H NMR (600 MHz, Methylene Chloride-*d*₂) δ 8.46 (dd, *J* = 7.5, 6.1 Hz, 2H), 7.85 (d, *J* = 7.4 Hz, 1H), 7.65 – 7.60 (m, 2H), 7.51-7.45, (m 2H), 7.38 (td, *J* = 7.5, 1.2 Hz, 1H), 7.34 (d, *J* = 7.9 Hz, 2H), 7.21 – 7.16 (m, 1H), 7.08 (s, 1H), 2.79 (m, 2H), 1.14 (dd, *J* = 6.9, 3.0 Hz, 12H). ¹³C NMR (151 MHz, Methylene Chloride-*d*₂) δ 146.2, 134.5, 132.8, 129.1, 126.4, 123.9, 123.6, 122.5, 119.8, 111.1, 106.7, 106.2, 28.9, 23.7. HR-MS (ESI) 493.1895 [M+Na⁺], calc. 493.1892 for C₃₂H₂₆N₂O₂Na.

(2) In a 25 mL Schlenk vessel **2** (50 mg, 0.106 mmol, 1 equiv.) and NBS (19 mg, 0.106 mmol, 1 equiv.) were mixed in anhydrous DMF (5 mL) in argon atmosphere for 24 hours in room temperature. After this time water (5 mL) was added, the precipitate was collected, dissolved in DCM and washed with water (20 mL) and brine (20 mL). Drying with Na₂SO₄ followed by evaporation of solvent gave a crude product **2** which was used in next step without further purification. (95%, 58 mg, orange solid). ¹H NMR (600 MHz, Chloroform-*d*) δ 8.50 (dd, *J* = 10.8, 7.3 Hz, 2H), 8.01 (d, *J* = 7.1 Hz, 1H), 7.60 (d, *J* = 7.9 Hz,

1H), 7.56 (d, $J = 7.9$ Hz, 1H), 7.49 – 7.40 (m, 3H), 7.32 (d, $J = 8.0$ Hz, 2H), 7.27 (t, $J = 7.6$ Hz, 1H), 2.78 (m, 2H), 1.19 – 1.14 (m, 12H). **HR-MS (APCI)** 549.1177 [$M+H^+$], calc. 549.1178 for $C_{32}H_{26}N_2O_2Br$.

(3a) To a 25 mL Schlenk vessel **3** (49 mg, 0.088 mmol, 1 equiv.) and 3,6-dit-butylcarbazole (30 mg, 0.106 mmol, 1.2 equiv.) were put with $Pd(PtBu_3)_2$ (6 mg, 0.01 mmol, 0.1 equiv.) and $NaOtBu$ (11 mg, 0.106 mmol, 1.2 equiv.) and dry on vacuum for 30 minutes. After this time toluene (2 mL) was added in argon atmosphere and the vessel was closed with a glass cap put to the oil bath to stir in $120^\circ C$. After 24 hours, the solvent was evaporated and the residue was subjected to a column chromatography (DCM/Hexane 2/1) to give product **4a** (43%, 22 mg, red solid). **1H NMR (500 MHz, Chloroform- d)** δ 8.59 (d, $J = 7.7$ Hz, 1H), 8.33 (d, $J = 7.5$ Hz, 1H), 8.26 (d, $J = 1.9$ Hz, 2H), 7.83 (d, $J = 8.1$ Hz, 1H), 7.65 (d, $J = 7.7$ Hz, 1H), 7.56 – 7.49 (m, 4H), 7.46 (t, $J = 7.8$ Hz, 1H), 7.32 (d, $J = 7.8$ Hz, 2H), 7.25 (d, $J = 7.7$ Hz, 2H), 7.22 (t, $J = 7.6$ Hz, 1H), 6.82 (d, $J = 7.5$ Hz, 1H), 2.78 (m, 2H), 1.51 (s, 18H), 1.16 (dd, $J = 10.6, 6.8$ Hz, 12H). **^{13}C NMR (125 MHz, Chloroform- d)** δ 163.6, 145.8, 144.0, 141.1, 137.8, 134.4, 133.9, 133.1, 131.6, 131.3, 129.4, 127.4, 124.2, 123.9, 123.1, 122.7, 122.2, 120.4, 118.4, 116.8, 116.3, 111.8, 110.9, 107.2, 34.9, 32.0, 29.0, 24.0. **HR-MS (APCI)** 748.3901 [M^+], calc 748.3903 for $C_{52}H_{50}N_3O_2$. **IR (cm^{-1})** 3358, 2955, 2924, 2853, 1707, 1650, 1592, 1443, 813, 753.

(3b) The compound was obtained according the same procedure as for **3a** with 10-dimethylacridine as the amine. (32%, red solid) **1H NMR (600 MHz, Methylene Chloride- d_2)** δ 8.58 (d, $J = 7.7$ Hz, 1H), 8.32 (d, $J = 7.4$ Hz, 1H), 7.85 (dt, $J = 8.2, 0.8$ Hz, 1H), 7.71 (d, $J = 7.7$ Hz, 1H), 7.60 (dd, $J = 7.7, 1.6$ Hz, 2H), 7.51 (m, 1H), 7.47 (t, $J = 7.8$ Hz, 1H), 7.35 (d, $J = 7.7$ Hz, 1H), 7.34 (d, $J = 7.7$ Hz, 3H), 7.17 (ddd, $J = 8.1, 7.2, 0.9$ Hz, 1H), 7.03 (td, $J = 7.4, 1.4$ Hz, 2H), 6.98 (ddd, $J = 8.7, 7.1, 1.6$ Hz, 2H), 6.77 (dd, $J = 8.2, 1.3$ Hz, 2H), 2.76 (p, $J = 6.8$ Hz, 2H), 1.83 (bs, 6H), 1.12 (dd, $J = 17.7, 6.8$ Hz, 12H). **^{13}C NMR (150 MHz, Methylene Chloride- d_2)** δ 146.2, 139.1, 134.5, 132.9, 131.1, 129.1, 127.2, 126.8, 125.5, 123.9, 122.8, 121.8, 121.7, 121.4, 113.9, 111.9, 107.5, 53.7, 53.6, 53.4, 53.2, 53.0, 28.9, 23.6. **HR-MS (APCI)** 678.3130 [M^+], calc 678.3121 for $C_{47}H_{40}N_3O_2$. **IR (cm^{-1})** 3063, 2959, 2924, 2853, 1707, 1650, 1592, 1445, 1419, 1335, 1232, 827, 750.

(3c) The compound was obtained according the same procedure as for **3a** with phenoxazine as the amine. (36%, deep-green-brown solid) **1H NMR (500 MHz, Chloroform- d)** δ 8.58 (d, $J = 7.7$ Hz, 1H), 8.43 (d, $J = 7.5$ Hz, 1H), 7.77 (d, $J = 8.1$ Hz, 1H), 7.61 (d, $J = 7.7$ Hz, 1H), 7.54 (t, $J = 8.0$ Hz, 2H), 7.51 – 7.43 (m, 2H), 7.32 (d, $J = 7.8$ Hz, 2H), 7.24 – 7.18 (m, 1H), 6.85 (dd, $J = 8.0, 1.5$ Hz, 2H), 6.77 (td, $J = 7.7, 1.5$ Hz, 2H), 6.64 (td, $J = 7.7, 1.5$ Hz, 2H), 6.39 (dd, $J = 8.1, 1.5$ Hz, 2H), 2.75 (m, 2H), 1.15 (dd, $J = 9.8, 6.9$ Hz, 12H). **^{13}C NMR (125 MHz, Chloroform- d)** δ 163.6, 145.8, 144.3, 134.5, 134.2, 133.2, 131.6, 131.2, 129.6, 129.4, 127.2, 127.1, 123.9, 123.7, 122.9, 122.6, 122.11, 122.07, 121.2, 116.6, 116.2, 114.0, 111.8, 107.4, 29.1, 24.0. **HR-MS (APCI)** 652.2596 [M^+], calc 652.2600 for $C_{44}H_{34}N_3O_3$. **IR (cm^{-1})** 3359, 3060, 2956, 2924, 2853, 1707, 1674, 1591, 1486, 1444, 1335, 1169, 742.

NMR spectra of main products

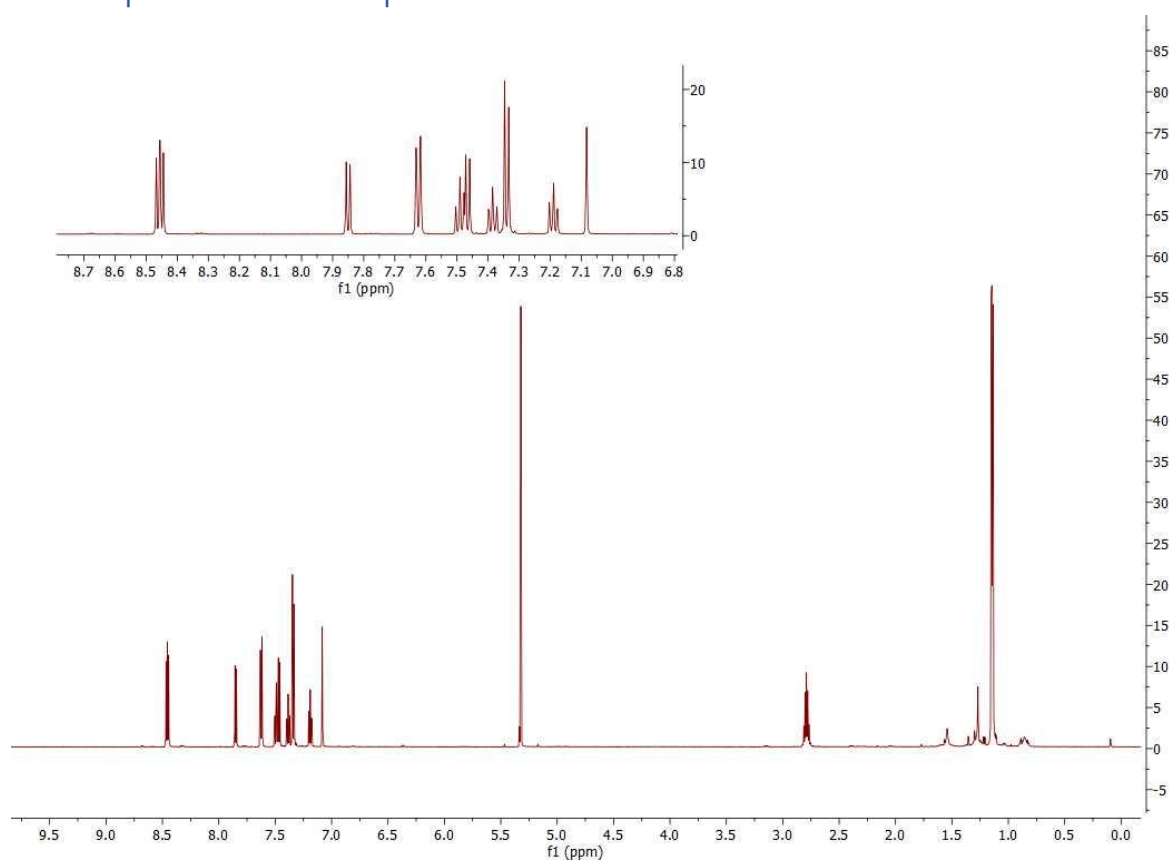


Figure S1. ^1H NMR spectrum of **1** (500 MHz, 300 K, CD_2Cl_2).

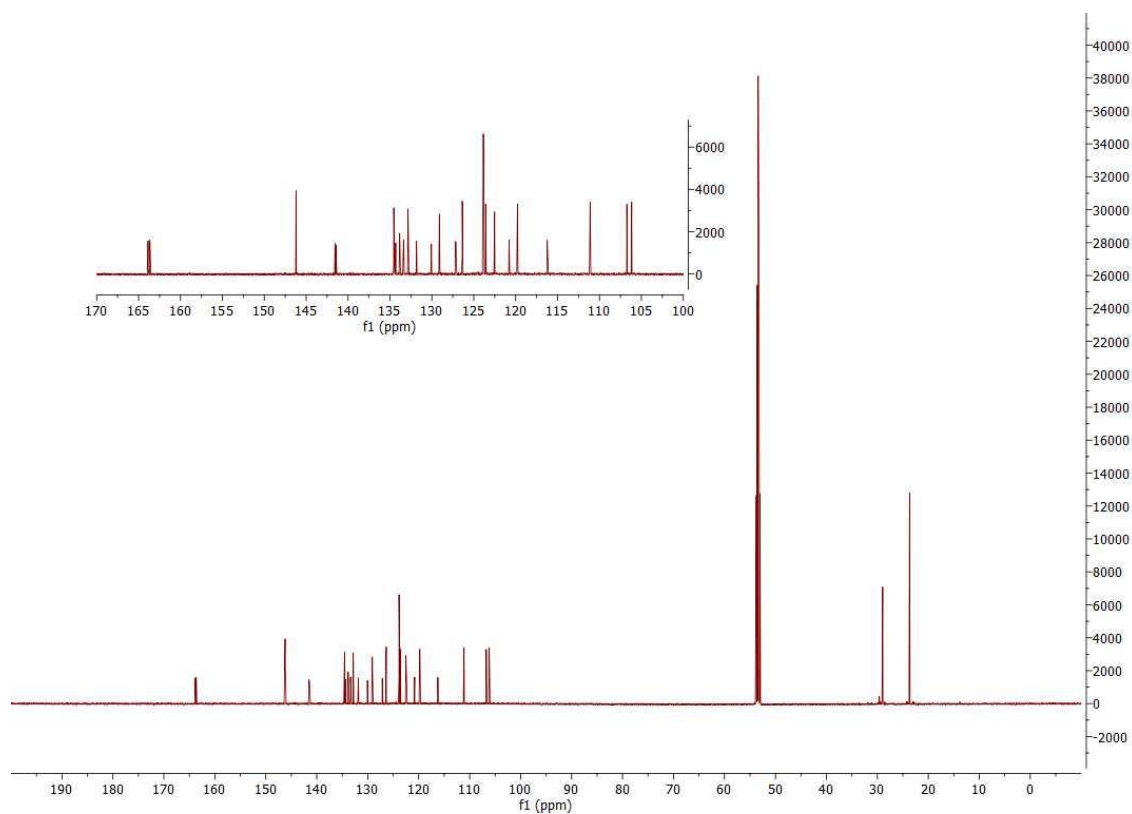


Figure S2. ^{13}C NMR spectrum of **1** (125 MHz, 300 K, CD_2Cl_2).

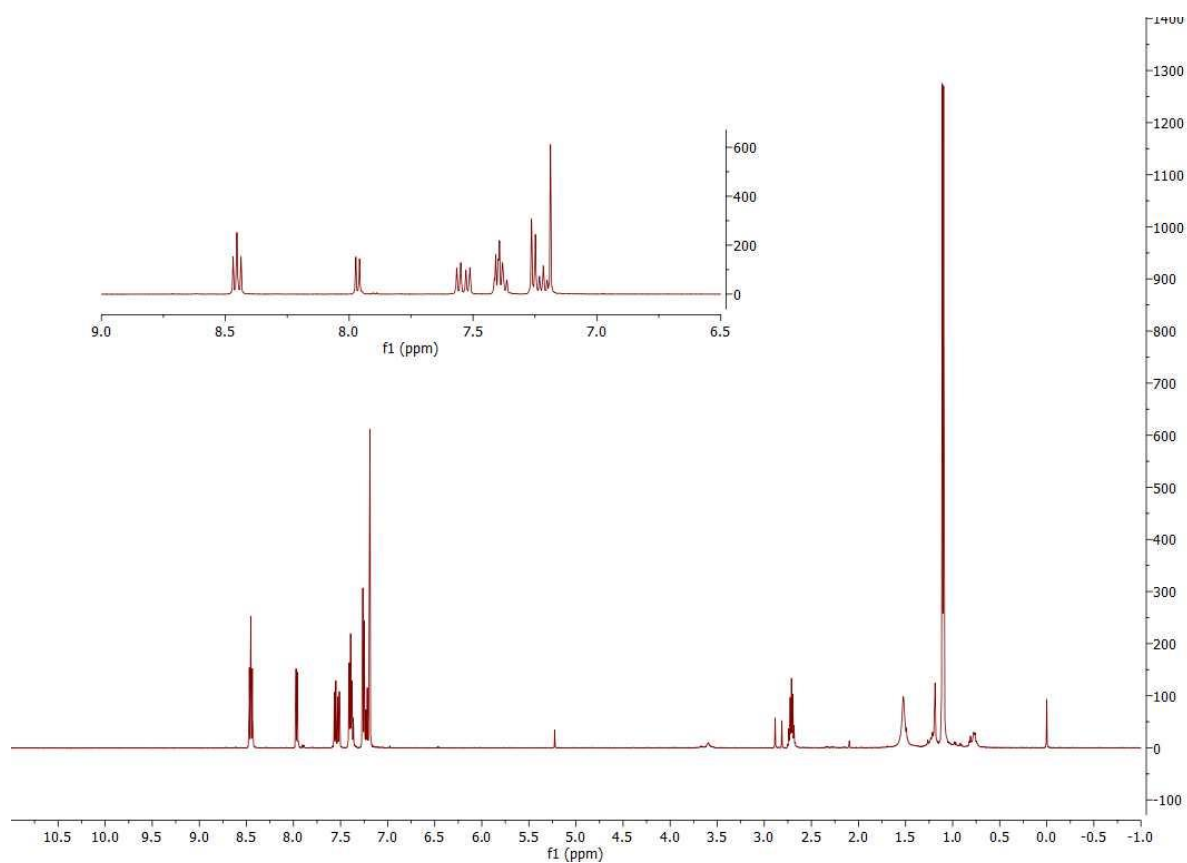


Figure S3. ^1H NMR spectrum of **2** (500 MHz, 300 K, CD_2Cl_2).

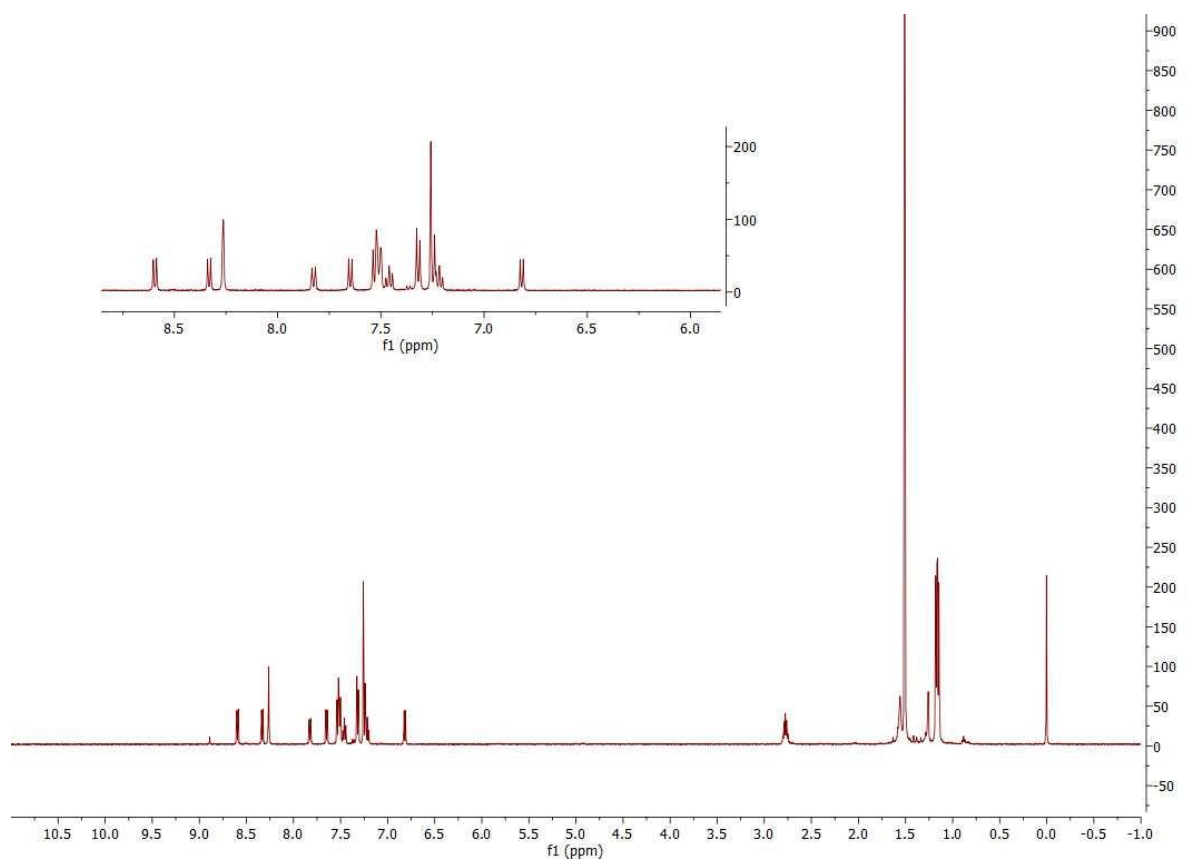


Figure S4. ^1H NMR spectrum of **3a** (500 MHz, 300 K, CDCl_3).

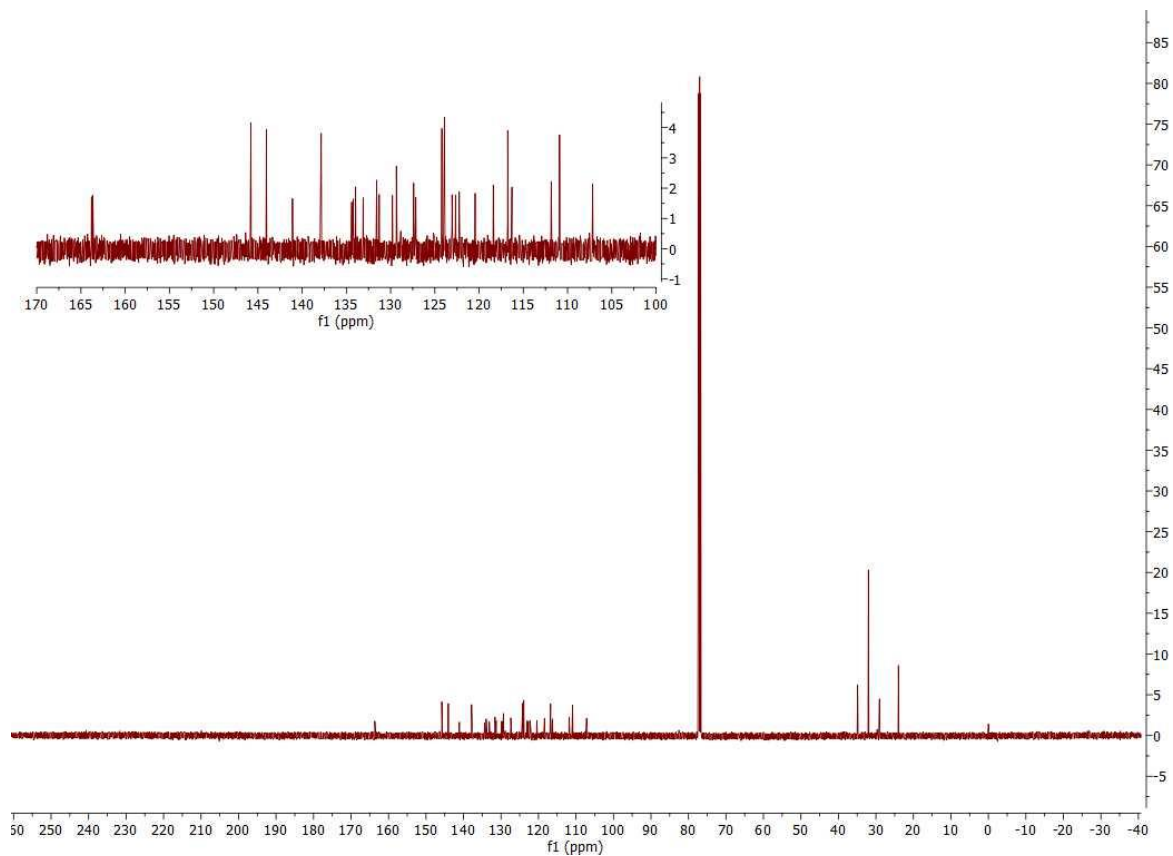


Figure S5. ^{13}C NMR spectrum of **3a** (125 MHz, 300 K, CDCl_3).

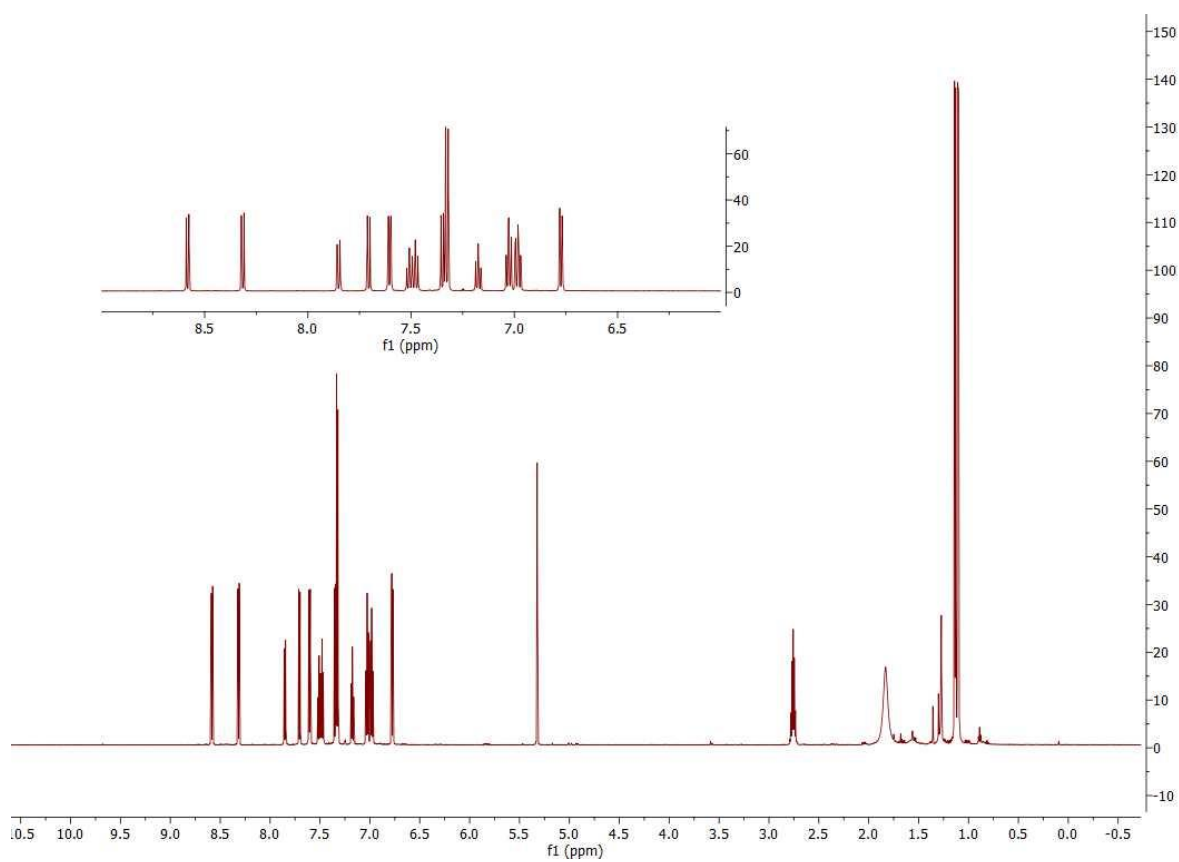


Figure S6. ^1H NMR spectrum of **3b** (500 MHz, 300 K, CD_2Cl_2).

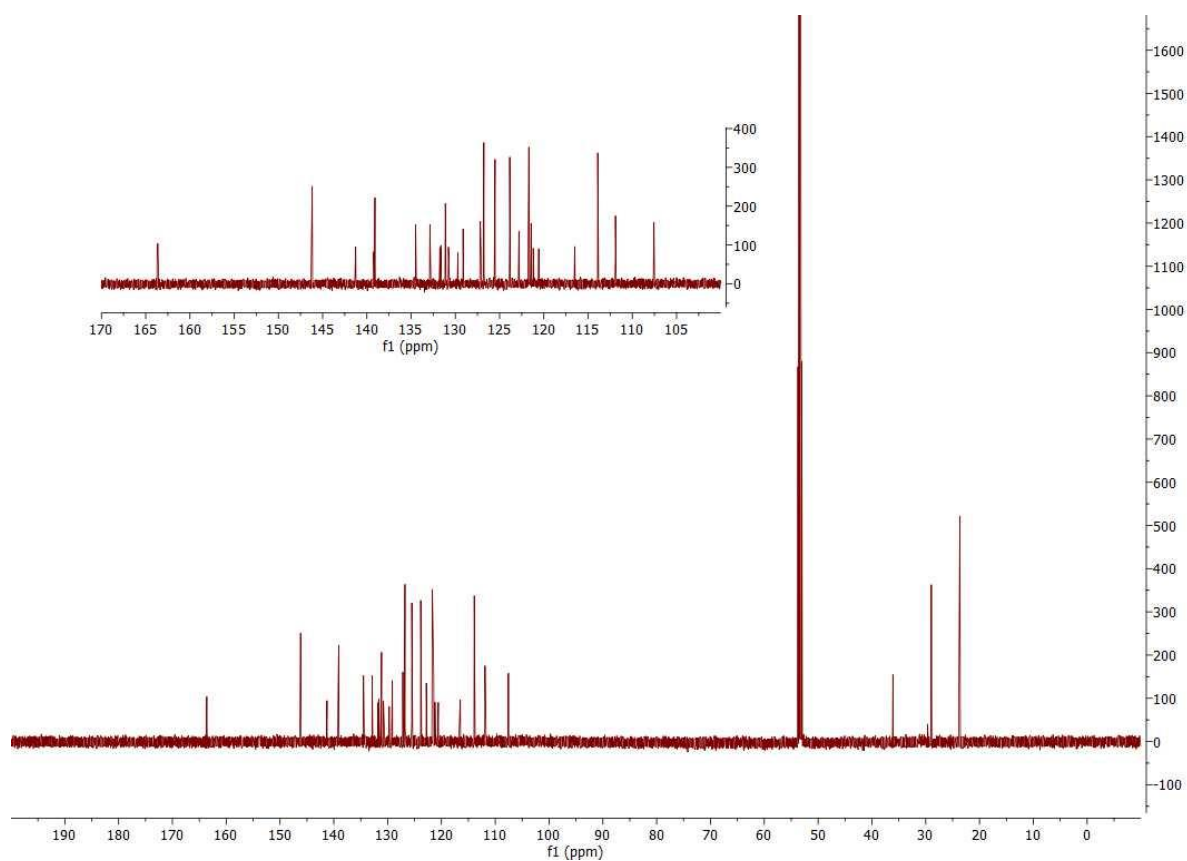


Figure S7. ^{13}C NMR spectrum of **3b** (125 MHz, 300 K, CD_2Cl_2).

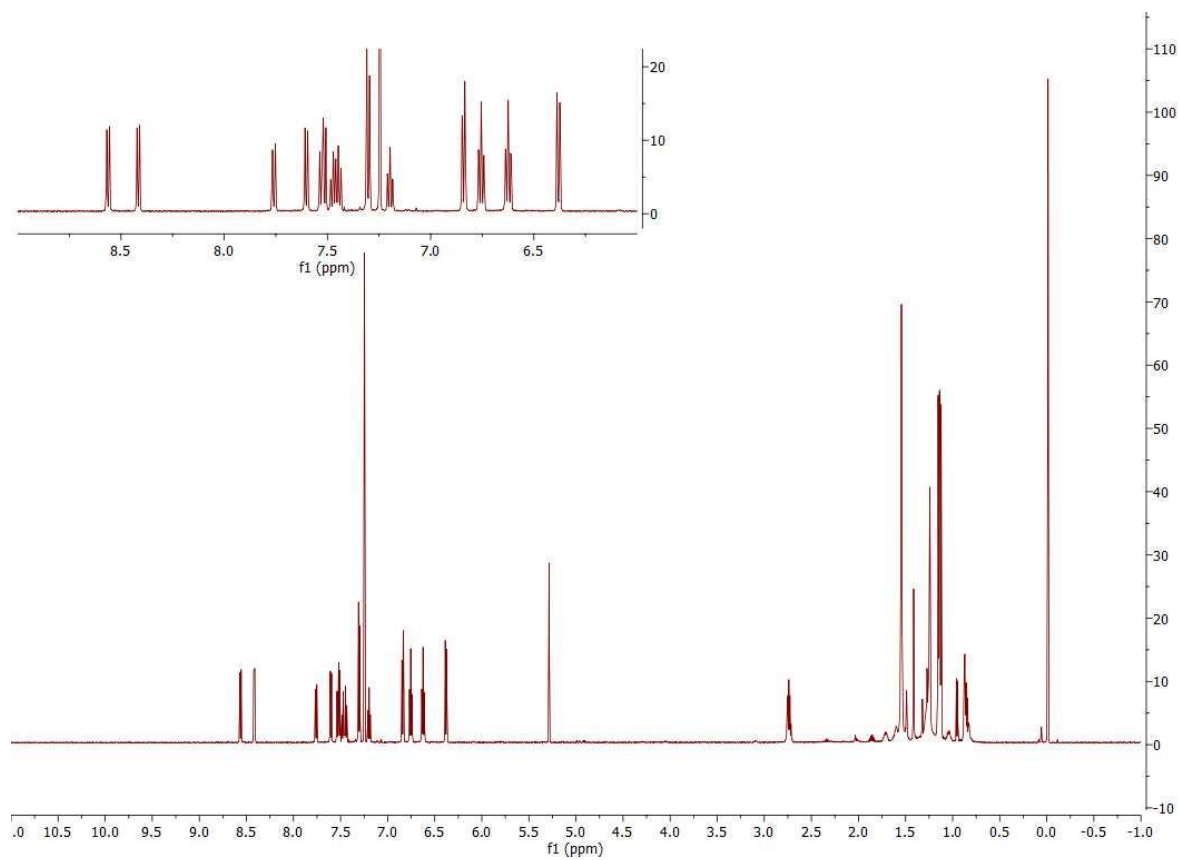


Figure S8. ^1H NMR spectrum of **3c** (500 MHz, 300 K, CDCl_3).

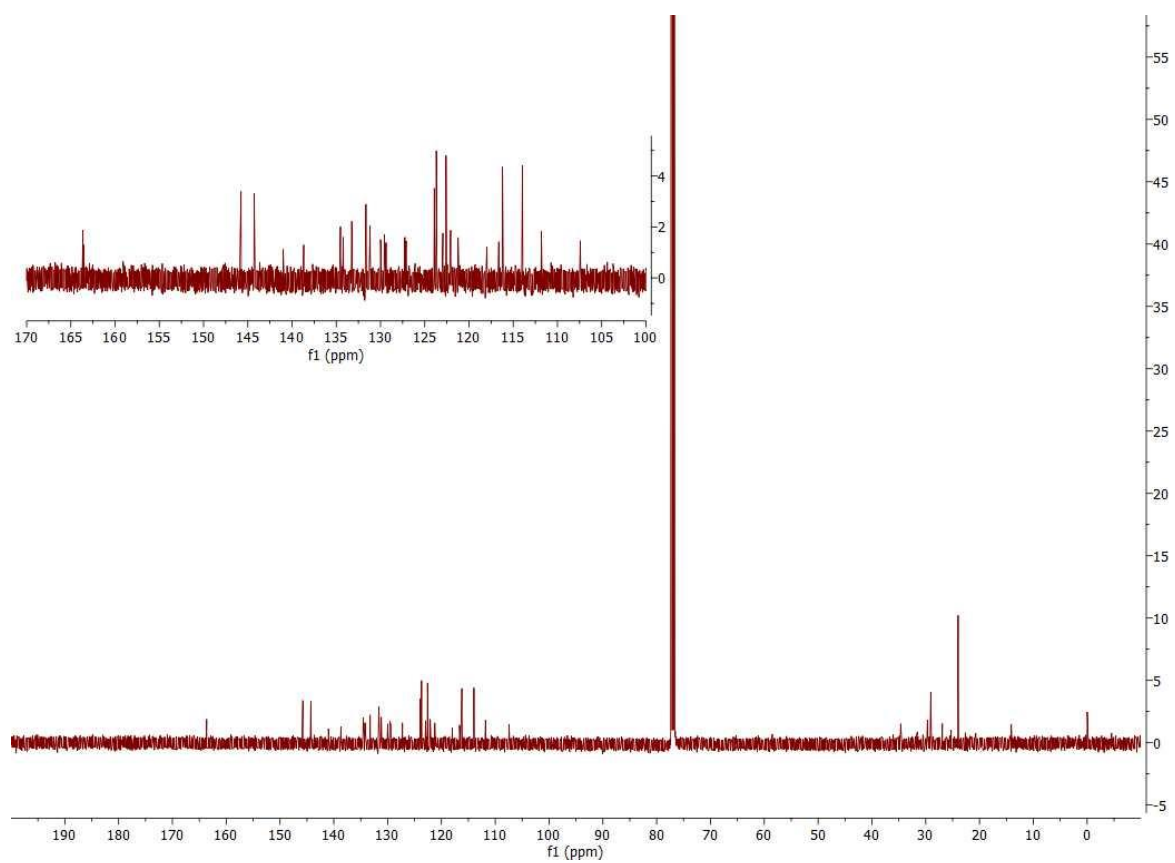


Figure S9. ^{13}C NMR spectrum of **3c** (150 MHz, 300 K, CDCl_3).

DFT analysis

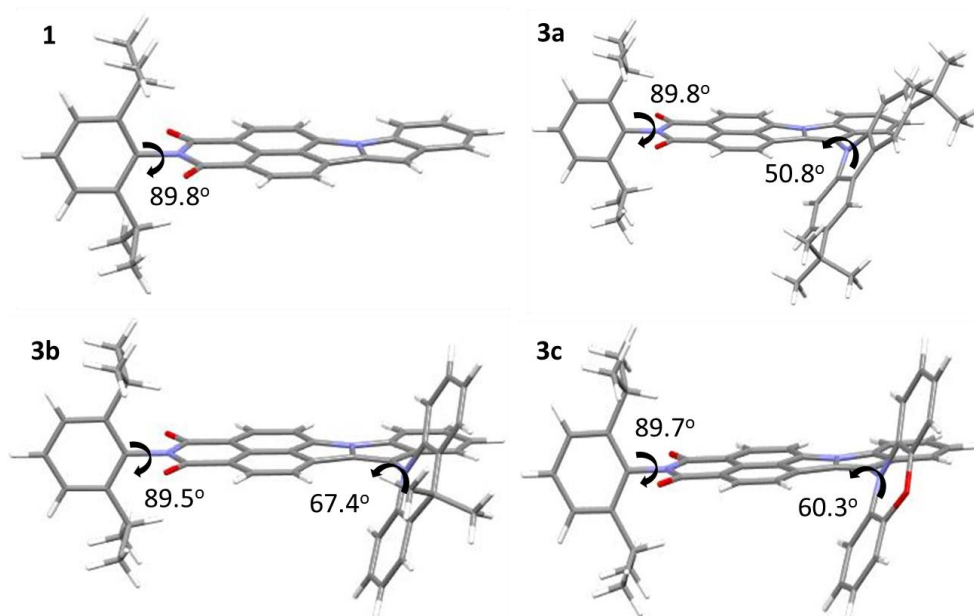


Figure S10. Optimized molecular structure of **1**, **3a**, **3b** and **3c** by DFT with twisted angle between electron deficient (acceptor) (NAI) and electron rich (donor) moiety.

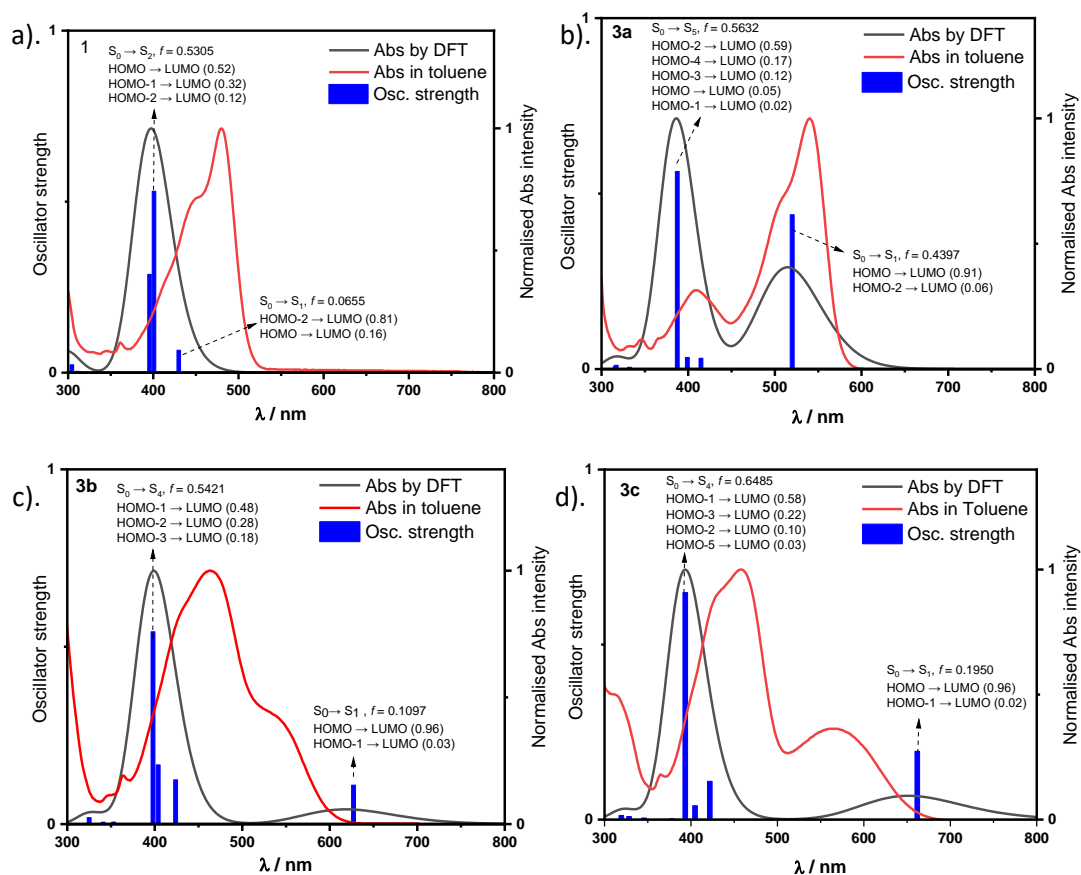
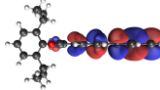
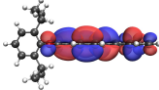
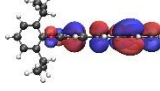
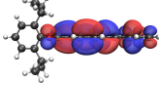
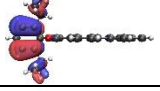
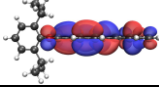
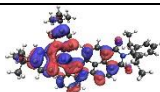
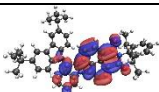
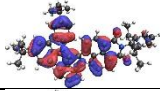
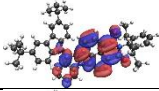
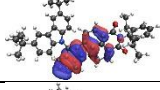
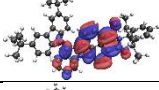
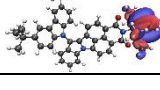
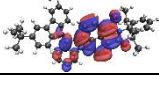
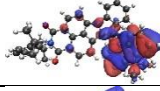
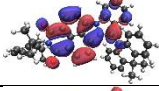
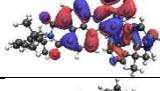
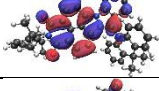
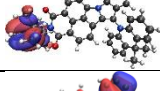
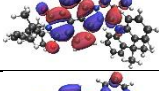
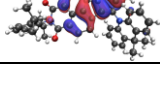
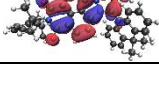
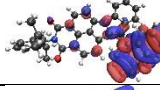
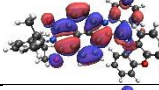
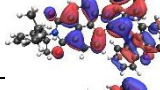
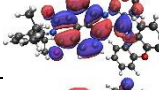
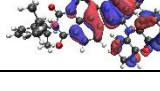
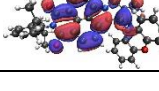


Figure S11. TDA-DFT simulation and experimental UV-Vis absorption in the gas phase of (a) **1**, (b) **3a** (c) **3b** and (d) **3c**.

Table S1. Excitation energy, composition, and density plots of dominant molecular orbital transitions of **1**, **3a**, **3b**, and **3c** (isovalue = 0.02).

Excited state	Energy / eV	Oscillator strength	Dominant orbital transition	Corresponding occupied orbital	Corresponding unoccupied orbital
1					
S1	2.88	0.0655	HOMO-2 → LUMO (0.81)		
S2	3.09	0.5305	HOMO → LUMO (0.52)		
			HOMO-1 → LUMO (0.32)		
3a					
S1	2.38	0.4397	HOMO → LUMO (0.91)		
S5	3.20	0.5632	HOMO-2 → LUMO (0.59)		
			HOMO-4 → LUMO (0.17)		
			HOMO-3 → LUMO (0.12)		
3b					
S1	1.97	0.1097	HOMO → LUMO (0.96)		
S4	3.11	0.5421	HOMO-1 → LUMO (0.48)		
			HOMO-2 → LUMO (0.28)		
			HOMO-3 → LUMO (0.18)		
3c					
S1	1.87	0.1950	HOMO → LUMO (0.96)		
S4	3.15	0.6485	HOMO-1 → LUMO (0.58)		
			HOMO-3 → LUMO (0.22)		

Electrochemistry and photophysics

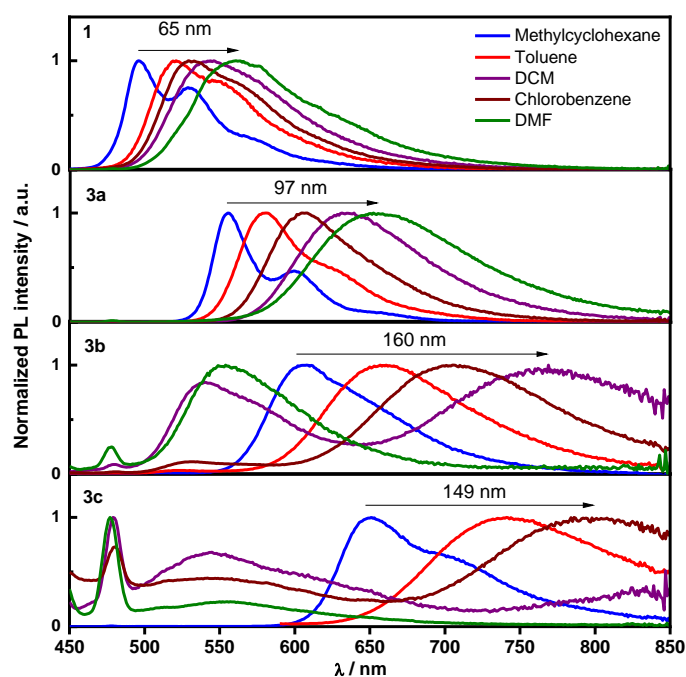


Figure S122. Photoluminescence spectra of **1**, **3a**, **3b** and **3c** in various solvents ($\lambda_{exc} = 420$ nm).

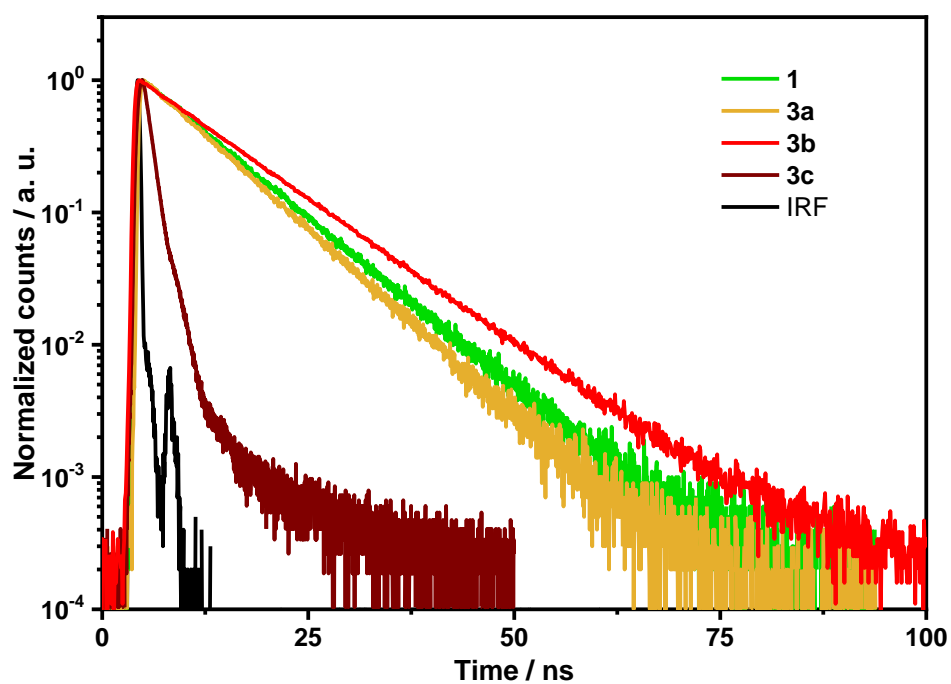


Figure S133. Time-resolved PL decays (TCSPC) of **1**, **3a**, **3b**, and **3c** in toluene. IRF is the instrument response function ($\lambda_{exc} = 374$ nm).

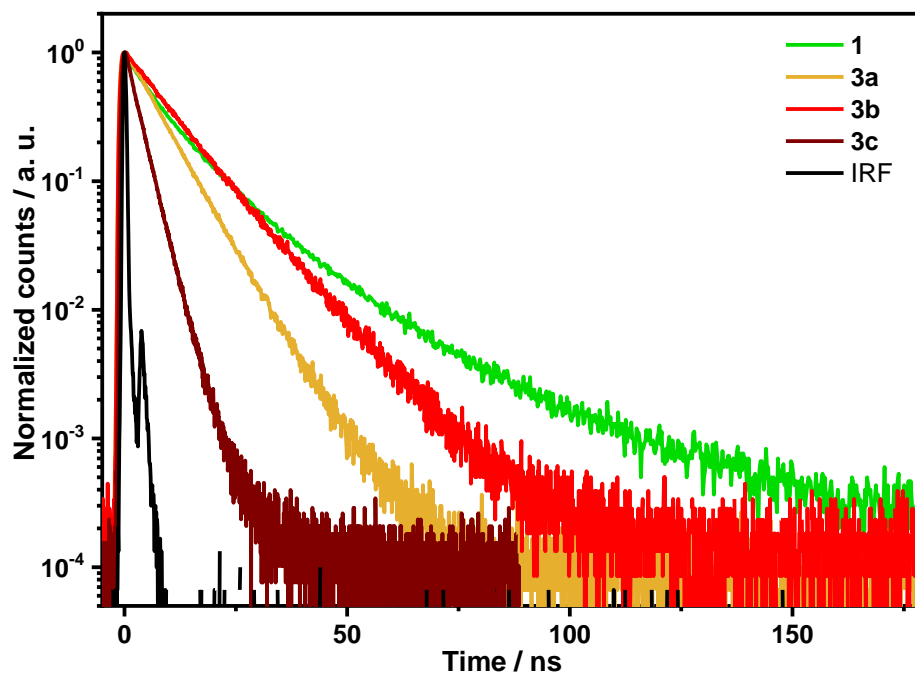


Figure S14. Time-resolved PL decays (TCSPC) of 5 wt% doped films in CBP of **1**, **3a**, **3b**, and **3c**. IRF is the instrument response function ($\lambda_{exc} = 374$ nm).

X-Ray

Table S2. Crystallographic data of compounds **1** and **3c**.

Name	1	3c
CCDC number	2290709	2290710
Empirical formula	C ₃₃ H ₂₈ N ₂ O ₂ Cl ₂	C ₄₆ H ₃₇ Cl ₄ N ₃ O ₃
Formula weight	555.47	821.58
Temperature/K	296(2)	296(2)
Crystal system	triclinic	monoclinic
Space group	P-1	P2 ₁
a/Å	9.672(2)	8.696(3)
b/Å	12.189(3)	15.535(5)
c/Å	13.165(3)	15.750(5)
α/°	87.549(15)	90
β/°	80.714(15)	91.87(2)
γ/°	67.560(14)	90
Volume/Å ³	1415.3(6)	2126.6(12)
Z	2	2
ρ _{calc} /cm ³	1.303	1.283
μ/mm ⁻¹	2.320	2.873
F(000)	580.0	852.0
Crystal size/mm ³	0.54 × 0.259 × 0.147	0.315 × 0.27 × 0.264
Radiation	CuKα (λ = 1.54178)	CuKα (λ = 1.54178)
2θ range for data collection/°	6.804 to 137.534	5.614 to 137.432
Index ranges	-11 ≤ h ≤ 11, -14 ≤ k ≤ 14, -15 ≤ l ≤ 15	-9 ≤ h ≤ 8, -17 ≤ k ≤ 17, -18 ≤ l ≤ 19
Reflections collected	31074	36641
Independent reflections	4893 [R _{int} = 0.0787, R _{sigma} = 0.0962]	5893 [R _{int} = 0.0698, R _{sigma} = 0.0863]
Data/restraints/parameters	4893/0/372	5893/5/510
Goodness-of-fit on F ²	0.971	1.014
Final R indexes [I >= 2σ (I)]	R ₁ = 0.0975, wR ₂ = 0.1956	R ₁ = 0.0633, wR ₂ = 0.1696
Final R indexes [all data]	R ₁ = 0.1981, wR ₂ = 0.2405	R ₁ = 0.1170, wR ₂ = 0.1911
Largest diff. peak/hole / e Å ⁻³	0.28/-0.45	0.26/-0.31

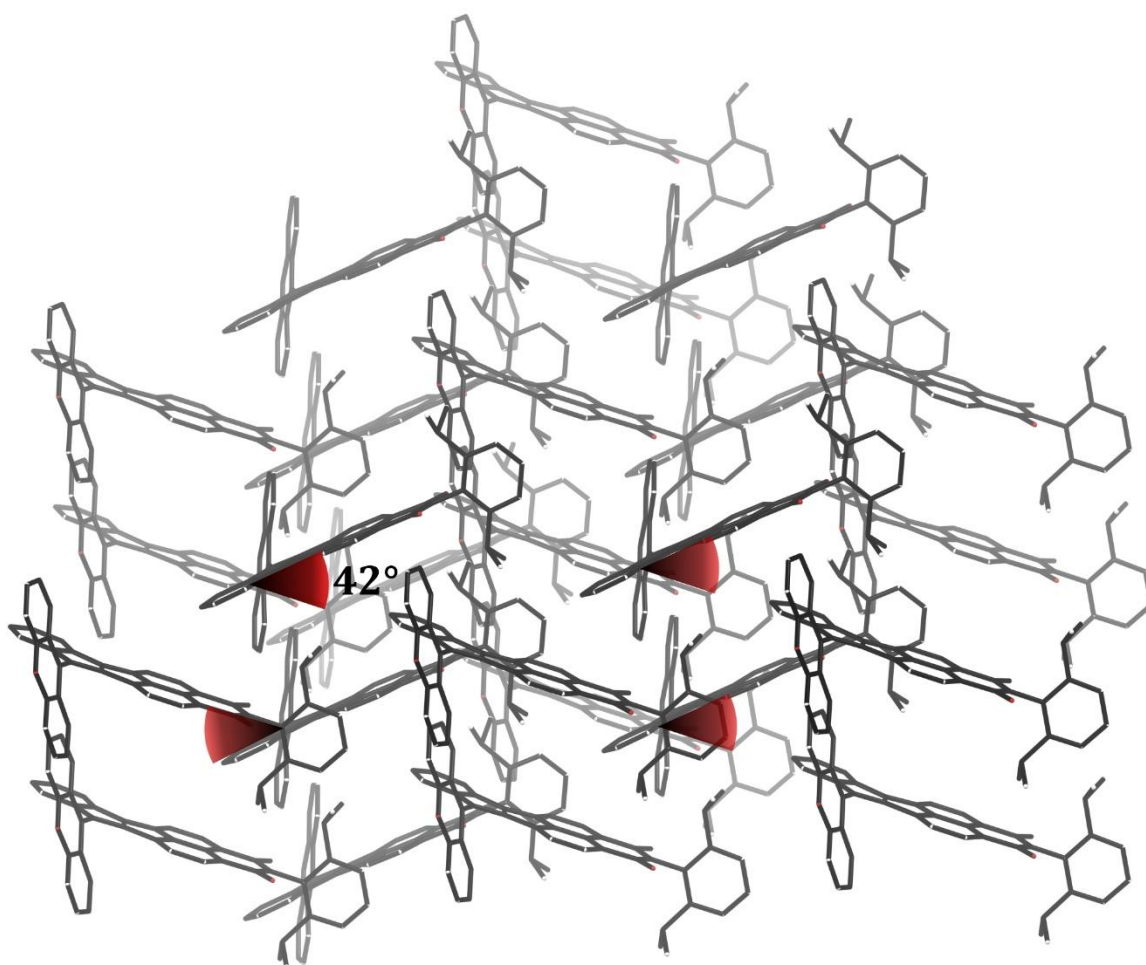


Figure S15. A packing of **3c** in crystal structure with indicated angles between planes of molecules in neighbourhood. Solvent molecules and hydrogen atoms were omitted for clarity.

MIDC analysis

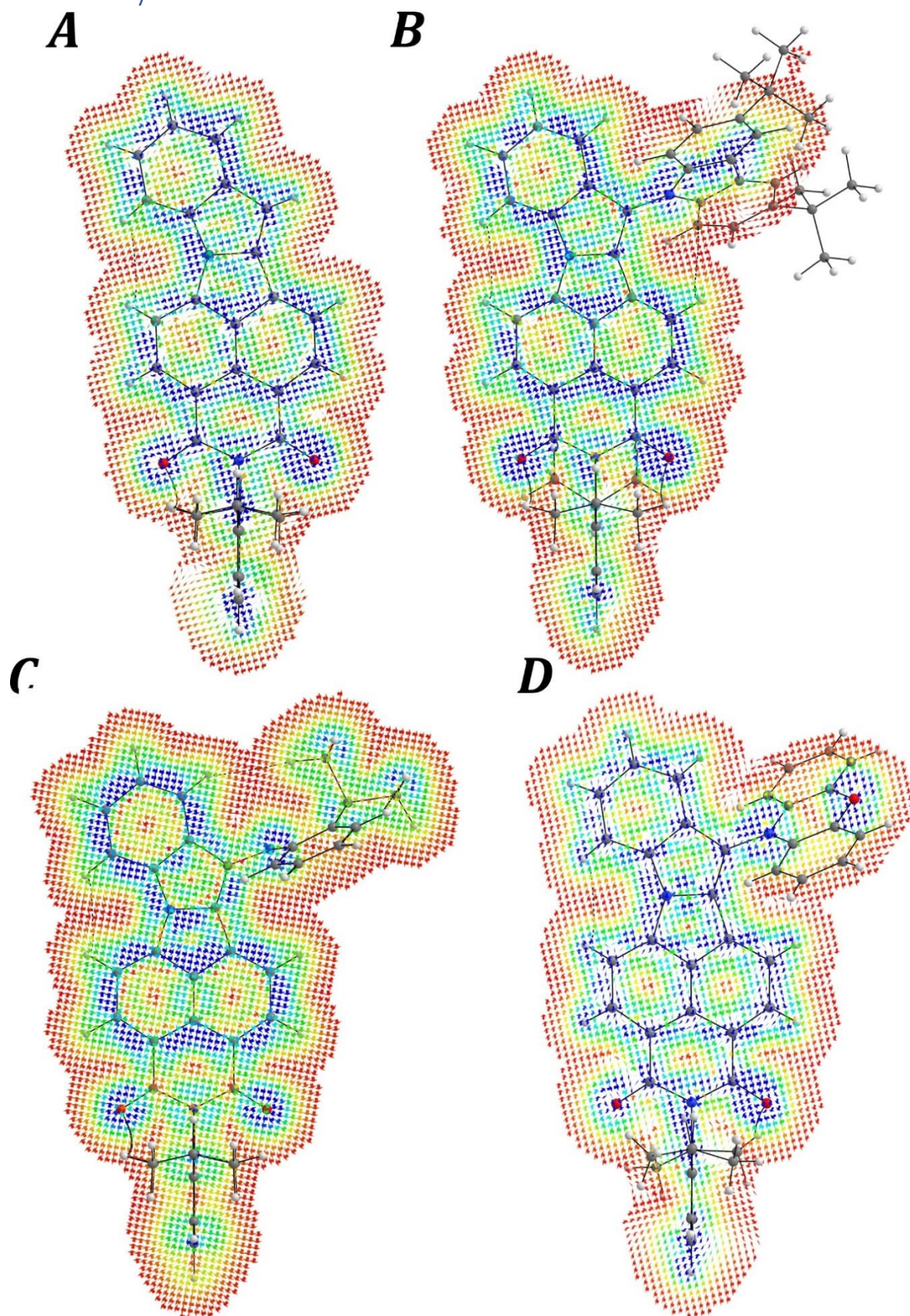


Figure S16. Visualization of the magnetically induced current density for **1** (A), **3a** (B), **3b** (C) and **3c** (D), 1 Å above the plane of PF-NAI moiety. Red color indicates weak current, blue – strong. The arrows show the direction of current flow. The magnetic field vector is directed perpendicular to the plane with the direction above the plane.

A magnetically induced current density (MICD) is a useful tool to predict a change of the delocalization paths within more complexed molecules where the conjugation of π electrons can be realized through different pathways. The intensity and the direction of current density vectors are both related to the effectiveness of conjugation. A proper description of electronic structure allows to make a prediction concerning properties driven from this phenomenon, e.g. absorption and emission. The more effectively delocalized system is the narrower band gap between HOMO and LUMO energy levels is and the bathochromic shift of absorption/emission is observed. An analysis of MICD calculated for **1** and **3c** (figure S17) showed a highly reduced global diatropic current for **1**. Both NI and pyrrolizine units communicate only by the C-N bond while the C(α)-C bond shows a weak diatropic current. A significant enhancement of π -electron communication after donor moiety (PXZ) introduction is noticed for **3c**. Such change can be driven by the presence of a nitrogen atom from the donor bonded to the C(β) atom of the pyrrolizine fragment. An electron donation caused by this structural motif stabilizes the delocalization within the acceptor which is realized as a strongly red-shifted emission. Thus, an exchange of donor can be a sufficient factor to modify a π cloud delocalization and tune the optical response of presented pyrrolizine based architectures.

References

- 1 W. Humphrey, A. Dalke and K. Schulten, *J Mol Graph*, 1996, **14**, 33–38.
- 2 N. M. O’Boyle and G. R. Hutchison, *Chem Cent J*, 2008, **2**, 24.
- 3 J. Stone, 1998.
- 4 J. D. Hunter, *Comput Sci Eng*, 2007, **9**, 90–95.
- 5 welcome to Mako!, <https://www.makotemplates.org/>, (accessed 9 October 2023).
- 6 <https://weasyprint.org>.
- 7 M. J. Frisch, G. W. Trucks, H. B. Schlegel, G. E. Scuseria, M. A. Robb, J. R. Cheeseman, G. Scalmani, V. Barone, G. A. Petersson, H. Nakatsuji, X. Li, M. Caricato, A. V. Marenich, J. Bloino, B. G. Janesko, R. Gomperts, B. Mennucci, H. P. Hratchian, J. V. Ortiz, A. F. Izmaylov, J. L. Sonnenberg, D. Williams-Young, F. Ding, F. Lipparini, F. Egidi, J. Goings, B. Peng, A. Petrone, T. Henderson, D. Ranasinghe, V. G. Zakrzewski, J. Gao, N. Rega, G. Zheng, W. Liang, M. Hada, M. Ehara, K. Toyota, R. Fukuda, J. Hasegawa, M. Ishida, T. Nakajima, Y. Honda, O. Kitao, H. Nakai, T. Vreven, K. Throssell, J. A. Montgomery Jr., J. E. Peralta, F. Ogliaro, M. J. Bearpark, J. J. Heyd, E. N. Brothers, K. N. Kudin, V. N. Staroverov, T. A. Keith, R. Kobayashi, J. Normand, K. Raghavachari, A. P. Rendell, J. C. Burant, S. S. Iyengar, J. Tomasi, M. Cossi, J. M. Millam, M. Klene, C. Adamo, R. Cammi, J. W. Ochterski, R. L. Martin, K. Morokuma, O. Farkas, J. B. Foresman and D. J. Fox, 2016.
- 8 C. Adamo and V. Barone, *J Chem Phys*, 1999, **110**, 6158–6170.
- 9 G. A. Petersson, T. G. Tensfeldt and J. A. Montgomery, *J Chem Phys*, 1991, **94**, 6091–6101.
- 10 S. Grimme, *Chem Phys Lett*, 1996, **259**, 128–137.
- 11 S. Hirata and M. Head-Gordon, *Chem Phys Lett*, 1999, **314**, 291–299.
- 12 T. G. S. Todd A. Keith, TK Gristmill Software, Overland Park KS, USA, 2019 (aim.tkgristmill.com).
- 13 A. D. Becke, *J Chem Phys*, 1997, **107**, 8554–8560.
- 14 N. G. Connelly and W. E. Geiger, *Chem Rev*, 1996, **96**, 877–910.
- 15 C. M. Cardona, W. Li, A. E. Kaifer, D. Stockdale and G. C. Bazan, *Adv Mater*, 2011, **23**, 2367–2371.
- 16 G. A. Crosby and J. N. Demas, *J Phys Chem*, 1971, **75**, 991–1024.
- 17 S. Fery-Forgues and D. Lavabre, *J Chem Educ*, 1999, **76**, 1260.
- 18 Nakamaru Katsumi, <https://doi.org/10.1246/bcsj.55.2697>, 2006, **55**, 2697–2705.
- 19 A. M. Brouwer, *Pure and Applied Chemistry*, 2011, **83**, 2213–2228.

- 20 N. C. Greenham, I. D. W. Samuel, G. R. Hayes, R. T. Phillips, Y. A. R. R. Kessener, S. C. Moratti, A. B. Holmes and R. H. Friend, *Chem Phys Lett*, 1995, **241**, 89–96.
- 21 K. Bartkowski, P. Zimmermann Crocomo, M. A. Kochman, D. Kumar, A. Kubas, P. Data and M. Lindner, *Chem Sci*, 2022, **13**, 10119–10128.